Supporting Information

Highly selective and sensitive fluorescent probe for Cu^{2+} based a novel naphthalimide-rhodamine platform and its application in live cell imaging

Chang Liu,[a] Xiaojie Jiao,[b] Song He,[b] Liancheng Zhao[a,b] and Xianshun Zeng*[a,b]

[a] School of Materials Science and Engineering, Institute of Information Functional Materials & Devices, Harbin Institute of Technology, Harbin 150001, China.

[b] Key Laboratory of Display Materials & Photoelectric Devices, Ministry of Education, School of Materials Science & Engineering, Tianjin University of Technology, Tianjin 300384, China.

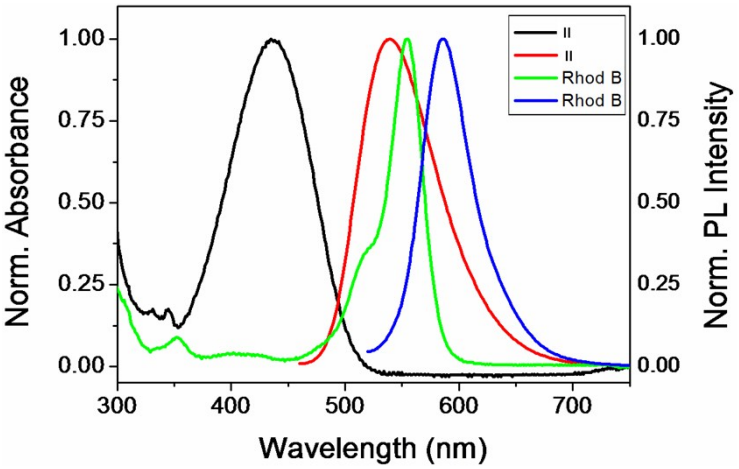

Chart S1 Normalized absorption and fluorescence spectra of model compounds **II** and rhodamine B (Rhod B). The fluorescence emission (red line) of naphthalimide derivative **II** is well overlapped with the absorption (green line) of rhodamine B.

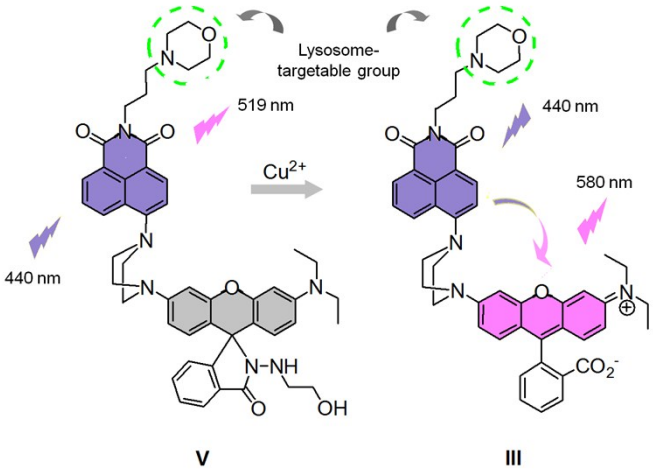

Scheme S1 Proposed reaction of Lyso-**V** with Cu^{2+}.

Table S1 Photophysical properties of dyes **III** and **IV** in different solvents.

Solvent / **III**	ε (M^{-1} cm^{-1})	λ_{abs} (nm)	λ_{em} (nm)	Φ
acetone	4366	350	521	0.40
$CHCl_3$	3900	352	516	0.76
DCM	3833	353	512	0.44
DMF	3833	348	527	0.40
DMSO	4066, 1466	357, 560	533	0.34
EtOAc	4566	347	512	0.63
EtOH	4066, 3933	360, 539	536	0.34
H_2O	3933, 3233	360, 550	549	0.076
MeOH	4300, 1700	342, 542	565	0.23
MeCN	4266	350	522	0.28
THF	4200	347	514	0.73
Solvent / **IV**	ε (M^{-1} cm^{-1})	λ_{abs} (nm)	λ_{em} (nm)	Φ
acetone	100666	557	514	0.16
$CHCl_3$	110000	558	507	0.51
DCM	117500	555	508, 590	0.20
DMF	99500	562	523	0.18
DMSO	104166	566	531	0.17
EtOAc	57666	561	508	0.20
EtOH	112833	556	530, 590	0.22
H_2O	86333	557	594	0.053
MeOH	119500	554	533, 590	0.15
MeCN	121833	551	516	0.14
THF	91500	560	510	0.23

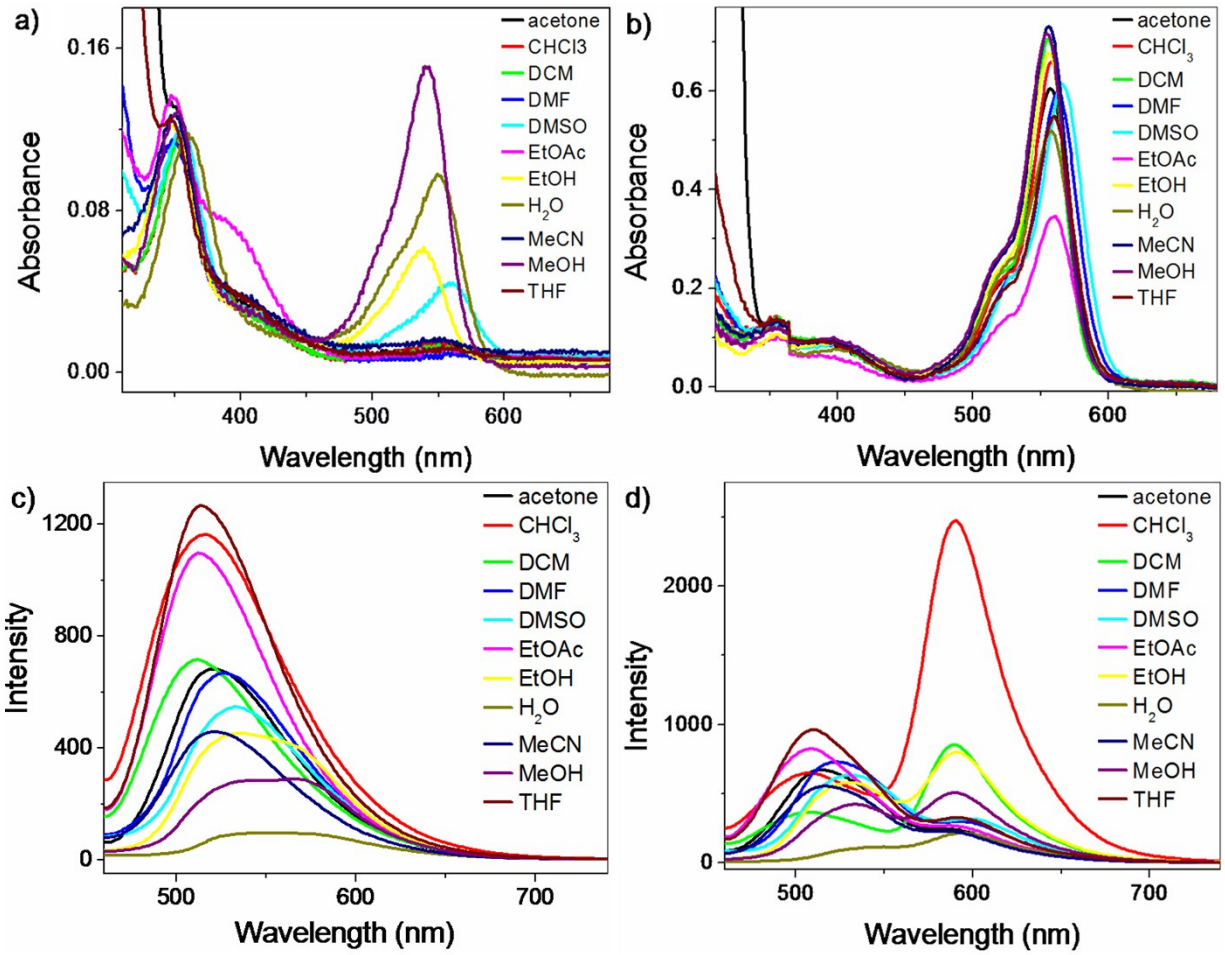

Fig. S1 a) and b) Absorption spectra of **III** (30 μM), **IV** (6 μM) in different solvents; c) and d) Emission spectra of **III**, **IV** (5 μM) in different solvents. λ_{ex} = 440 nm; slit: 5 nm, 10 nm.

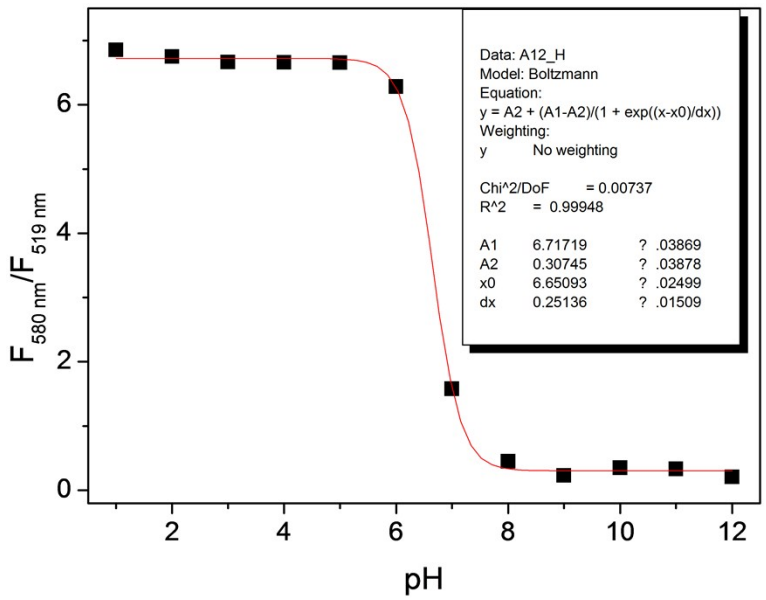

Fig. S2 $F_{580\ nm}/F_{519\ nm}$ for **III** (6 μM) as a function of pH from 1-12 in water. λ_{ex} = 440 nm; slit: 5 nm, 10 nm.

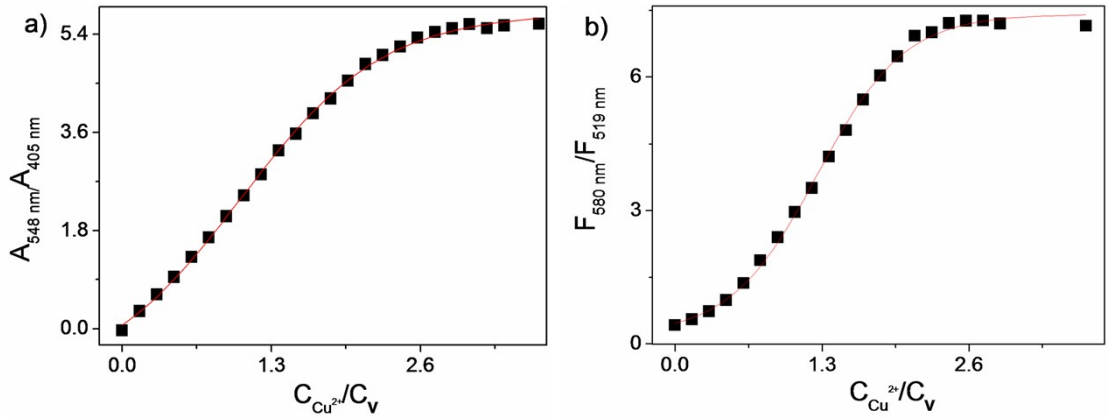

Fig. S3 a) $A_{548\ nm}/A_{405\ nm}$ for **V** as a function of C_{Cu}^{2+}/C_V from absorption titrations spectra of probe **V** (11 μM) in H_2O-MeCN (2:1, v/v); b) $F_{580\ nm}/F_{519\ nm}$ for **V** as a function of C_{Cu}^{2+}/C_V from fluorescence titrations spectra of probe **V** (5.5 μM) in H_2O-MeCN (2:1, v/v).

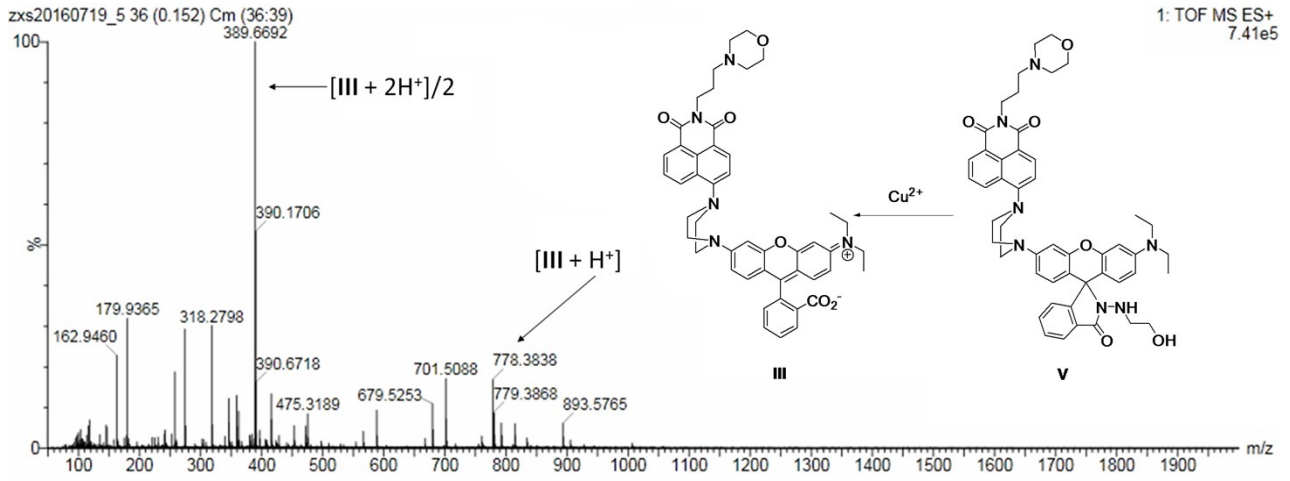

Fig. S4 HRMS spectra of **V** upon addition of Cu^{2+} (3.0 equiv.). The peaks (m/z) at 778.3838 and 389.6692 correspond to those of [**III** + H^+] (Calcd: 778.3601) and [**III** + $2H^+$]/2 (Calcd: 389.6836), respectively.

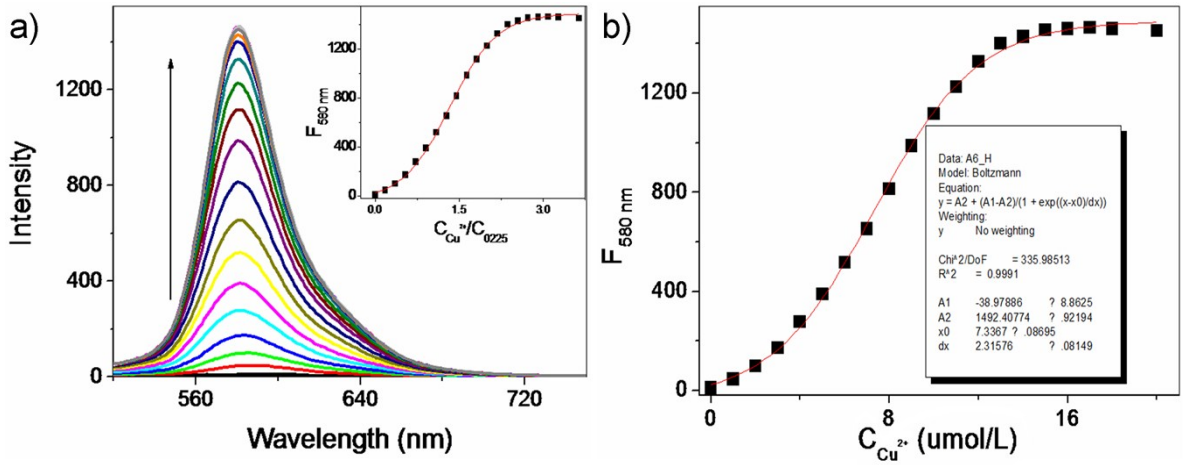

Fig. S5 a) Fluorescence titrations spectra of **V** (5.5 μM) in the presence of different concentrations of Cu^{2+} in H_2O-MeCN (2:1, v/v). λ_{ex} = 500 nm; slit = 5.0 nm, 10.0 nm; b) Measurement of the fluorescence turn-on constant ($K_{turn\text{-}on}$) of **V** (5.5 μM).[S1]

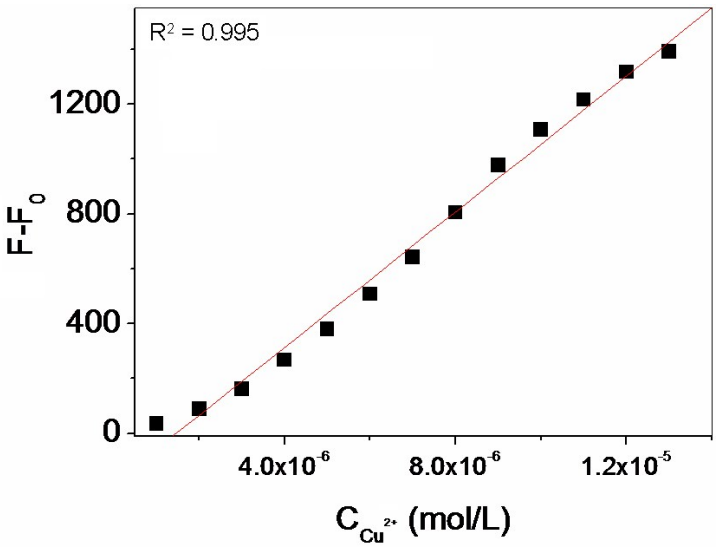

Fig. S6 The fluorescence intensity change ($\Delta F = F - F_0$) versus [Cu^{2+}]. The detection limit (DL) can be calculated with the equation[S2], DL = 3σ/M, where "M" is the calibration sensitivity of the fluorescence intensity change ($\Delta F = F - F_0$) versus [Cu^{2+}], and "σ" is the standard deviation of the blank signal (F_0) obtained without Cu^{2+}. From this, the detection limits of the probe for Cu^{2+} was found to be 1.45 nM under the testing conditions. ($\sigma = 0.06$, $M = 1.24 \times 10^8$)

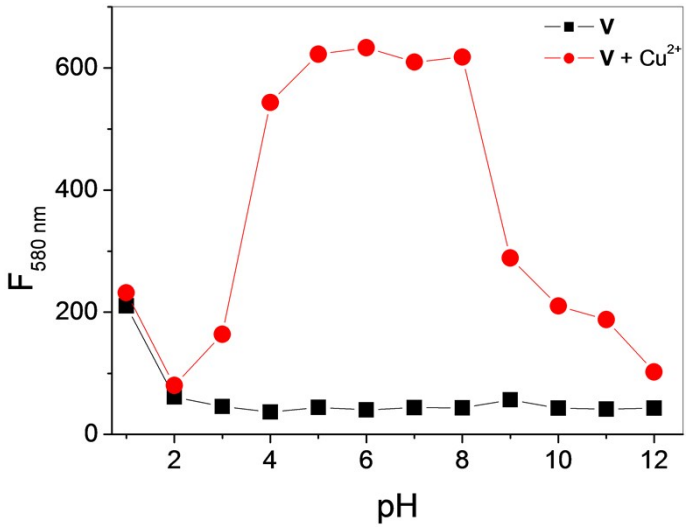

Fig. S7 Fluorescence intensities of **V** (5.5 μM) at 580 nm in the presence and absence of Cu^{2+} (3.0 equiv) at different pH.

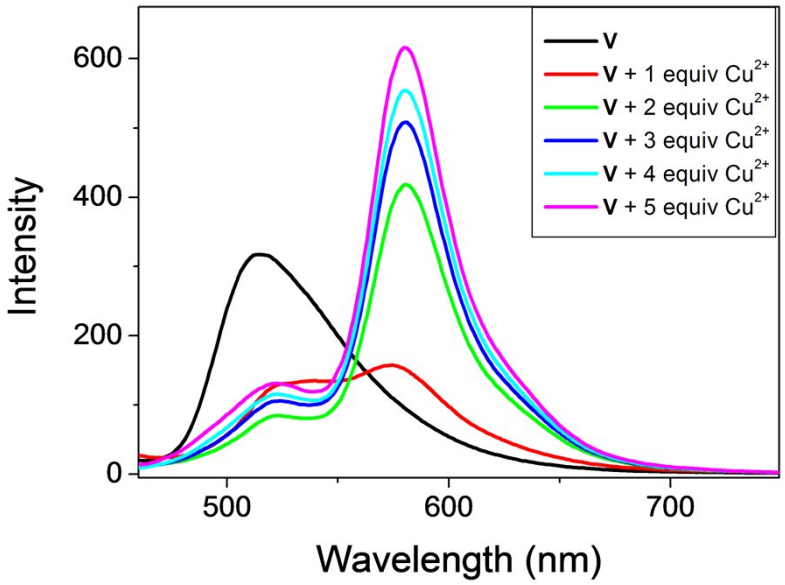

Fig. S8 The fluorescence responses of **V** (5.5 μM) toward Cu^{2+} (in the presence of 0, 1, 2, 3, 4, 5 equiv of Cu^{2+}, respectively) in the presence of fetal calf serum (FBS) (HEPES/FBS = 90 : 10), (10 mM, pH = 7.4, v/v). λ_{ex} = 440 nm; slit: 5 nm, 10 nm.

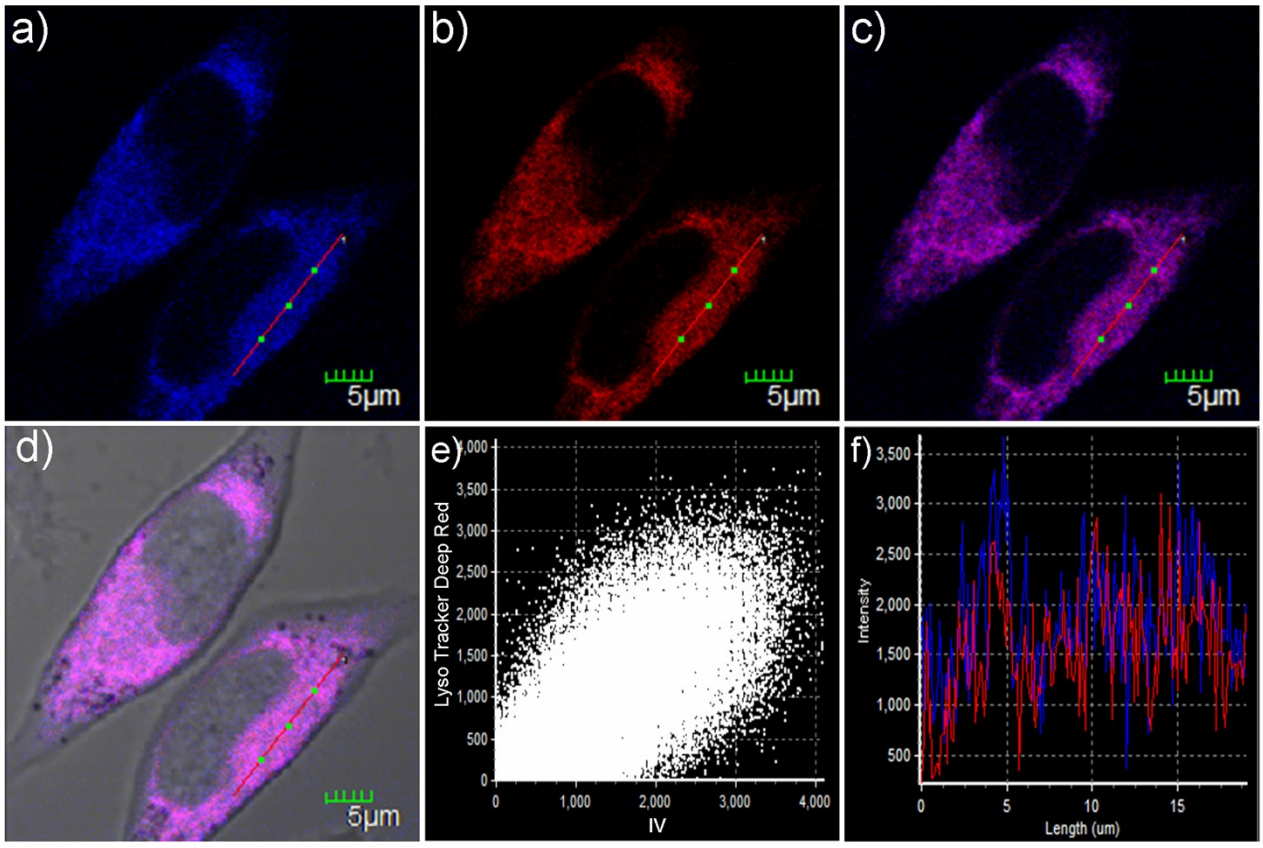

Fig. S9 Co-localization of LTDR and **IV** in L929 cells. Cells were co-stained with LTDR (100 nM) and **IV** (200 nM) at 37 ºC for 30 min. a) Image from the **IV** channel (λ_{ex} = 405 nm; λ_{em}: 502-545 nm); b) Image from the LTDR (λ_{ex} = 635 nm, λ_{em}: 650-706 nm); c) Merged image of a) and b); d) Merged image of a), b) and brightfield; e) Intensity correlation plot of LTDR and **IV**; f) Intensity profiles of LTDR and **IV** within the linear ROIs (red lines in a) and b)) across the L929 cell. Blue lines represent the intensity of the **IV** and red lines represent the intensity of LTDR.

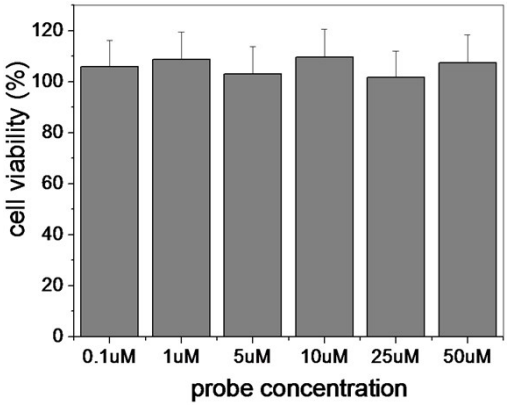

Fig. S10 MTT assays of **V** on L929 cells after an incubation time of 24 h at various dose concentrations (0.1 μM to 50 μM, 1% DMSO) at 37 °C.

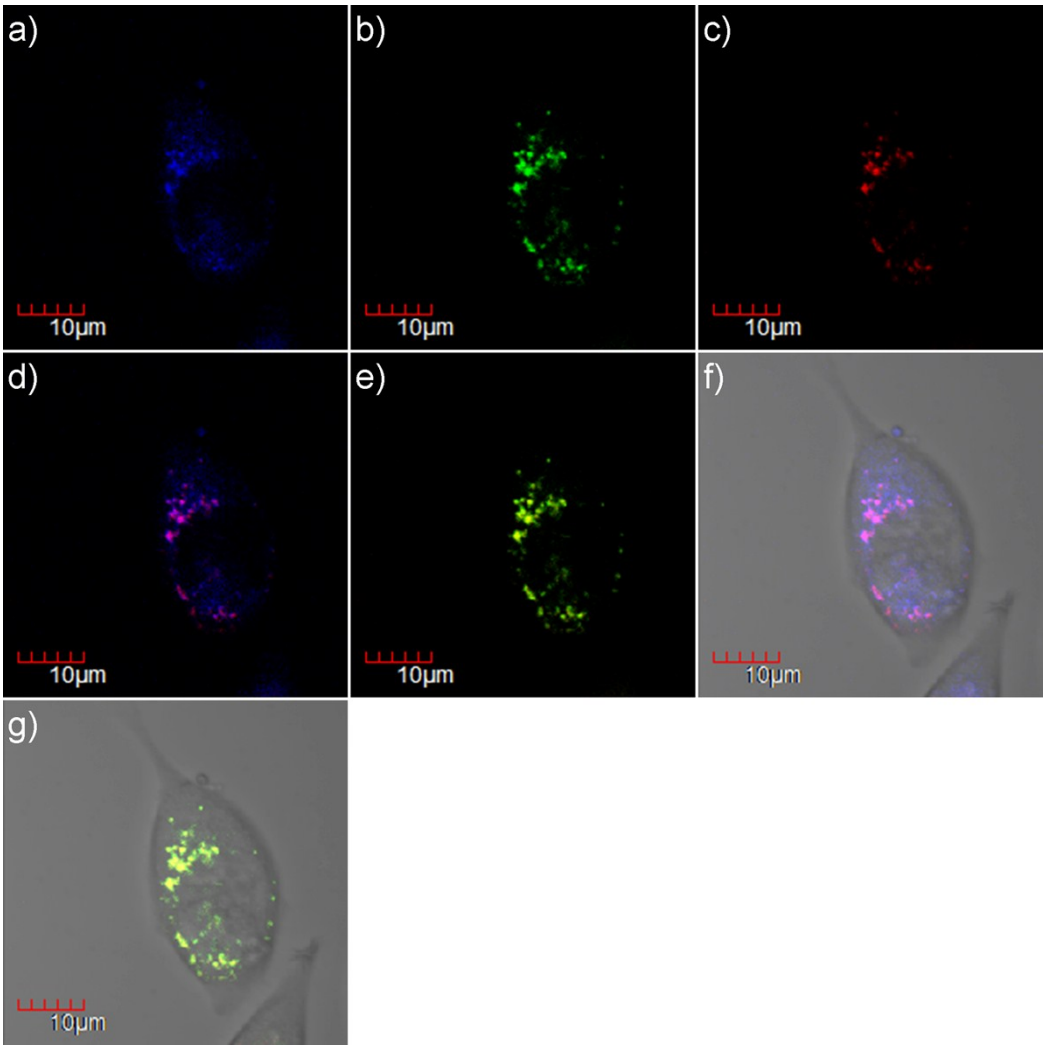

Fig. S11 Co-localization of LTDR and **V** in L929 cells. Cells were co-stained with LTDR (100 nM) and **V** (200 nM), and then treated with Cu^{2+} (1 μM) at 37 °C for 30 min. a) Image from the **V** channel (λ_{ex} = 405 nm, λ_{em}: 512-547 nm); b) Image from the **V** channel (λ_{ex} = 488 nm, λ_{em}: 581-620 nm); c) Fluorescence image from the LTDR (λ_{ex} = 635 nm, λ_{em}: 655-755 nm); d) Merged image of a) and c); e) Merged image of b) and c); f) Merged image of d) and brightfield; g) Merged image of e) and brightfield.

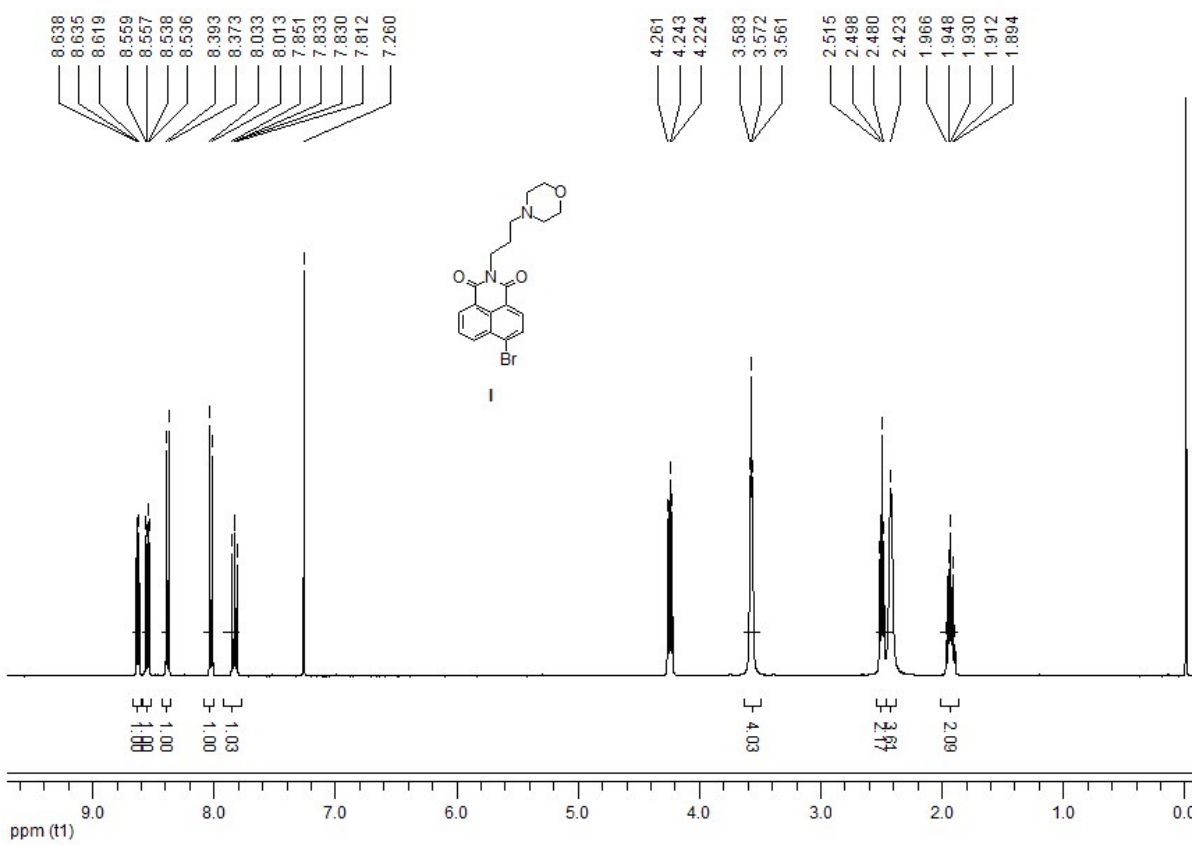

Fig. S12 ^{1}H NMR of **I** (400 MHz, $CDCl_3$).

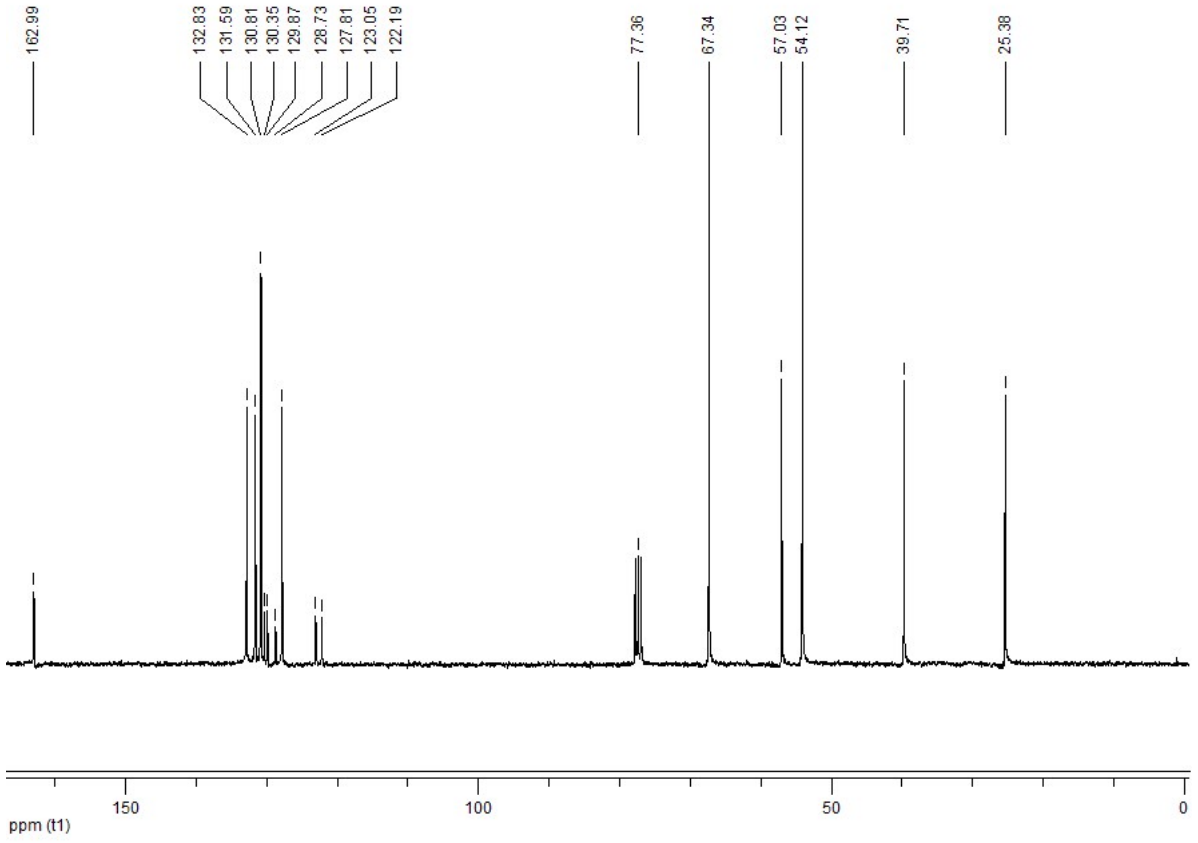

Fig. S13 ^{13}C NMR of **I** (75 MHz, $CDCl_3$).

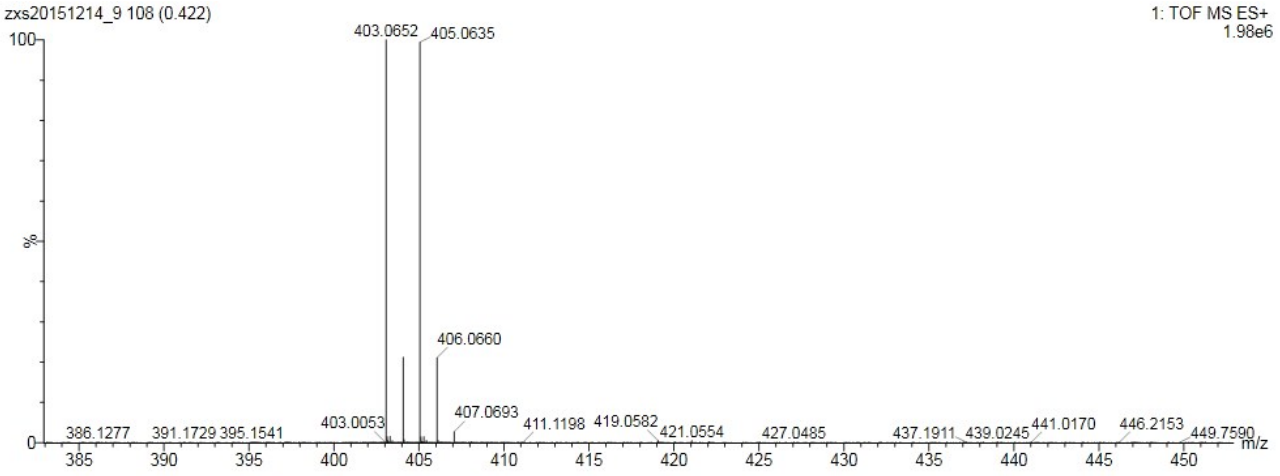

Fig. S14 HRMS (LC/MS) spectra of **I**. The peak at m/z = 403.0652 was assigned to the mass of [**I** + H^+].

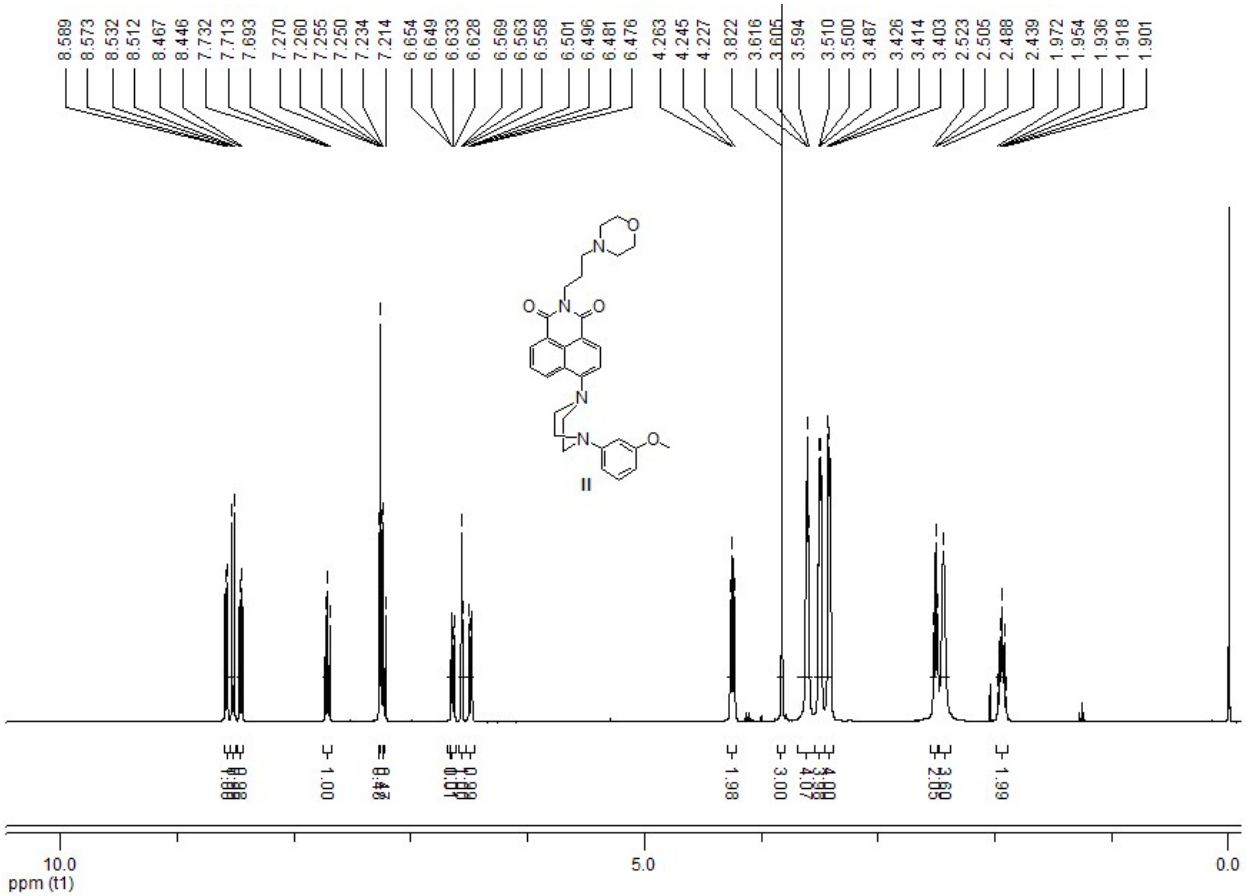

Fig. S15 ^{1}H NMR of **II** (400 MHz, $CDCl_3$).

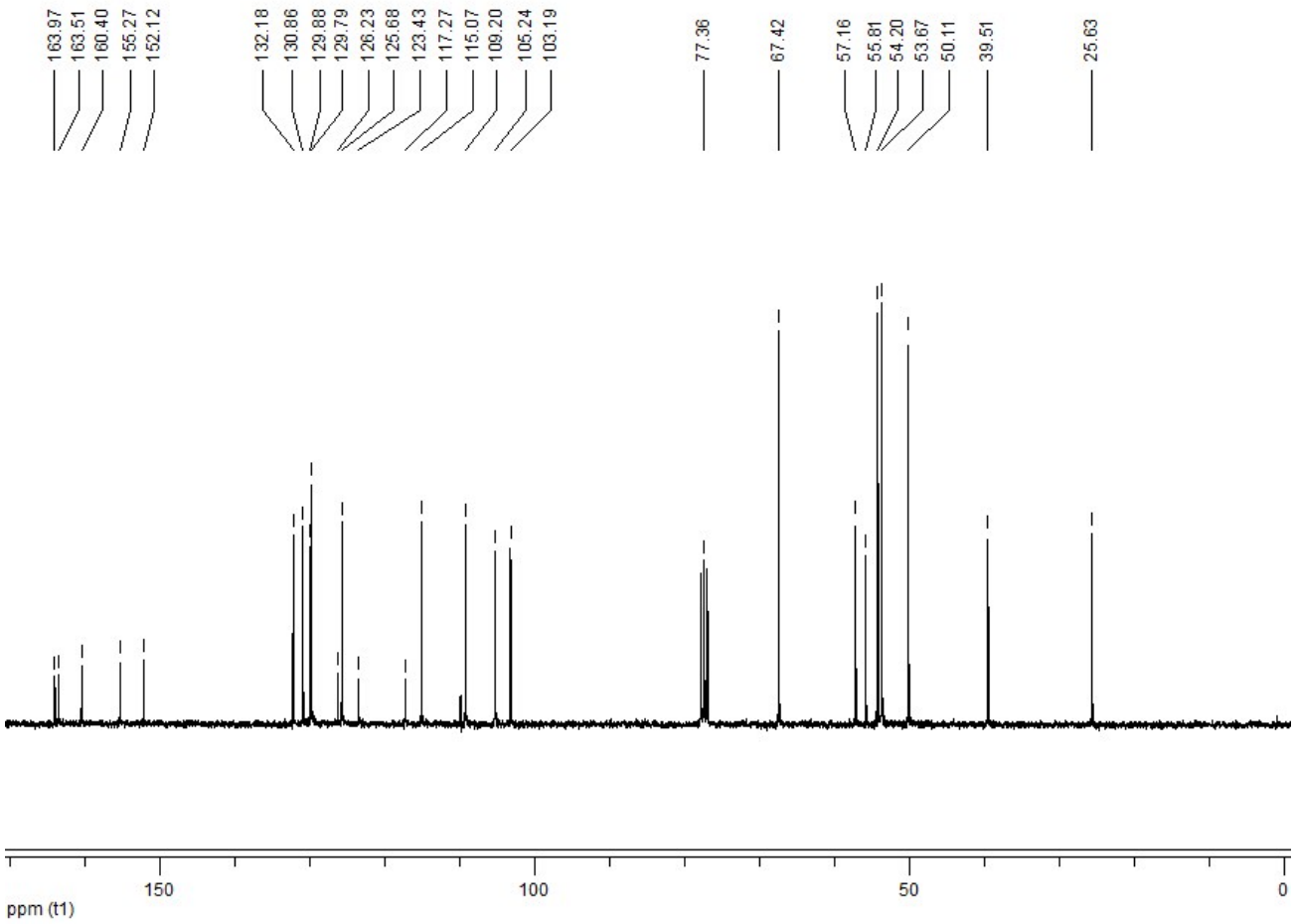

Fig. S16 ^{13}C NMR of **II** (75 MHz, $CDCl_3$).

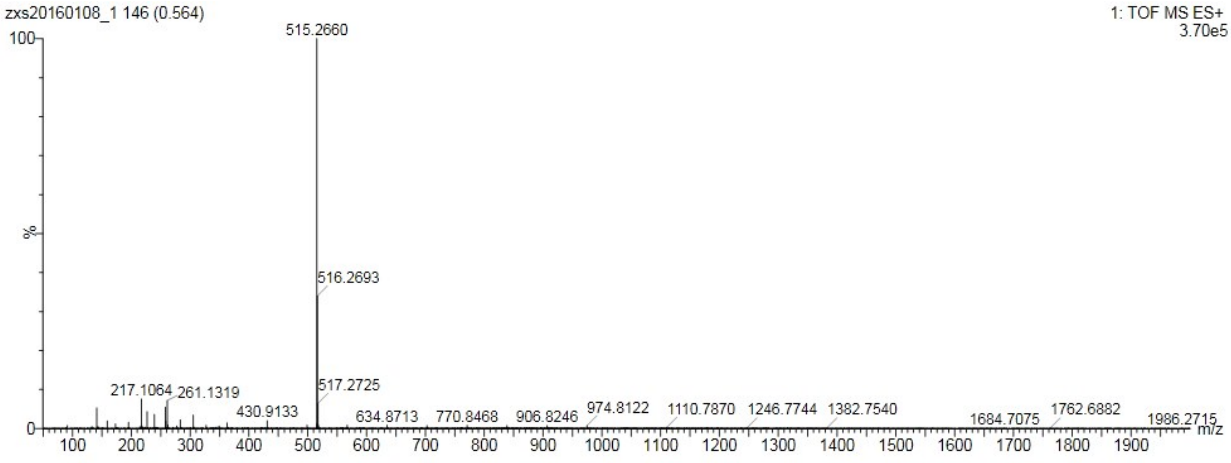

Fig. S17 HRMS (LC/MS) spectra of **II**. The peak at m/z = 515.2660 was assigned to the mass of [**II** + H^+].

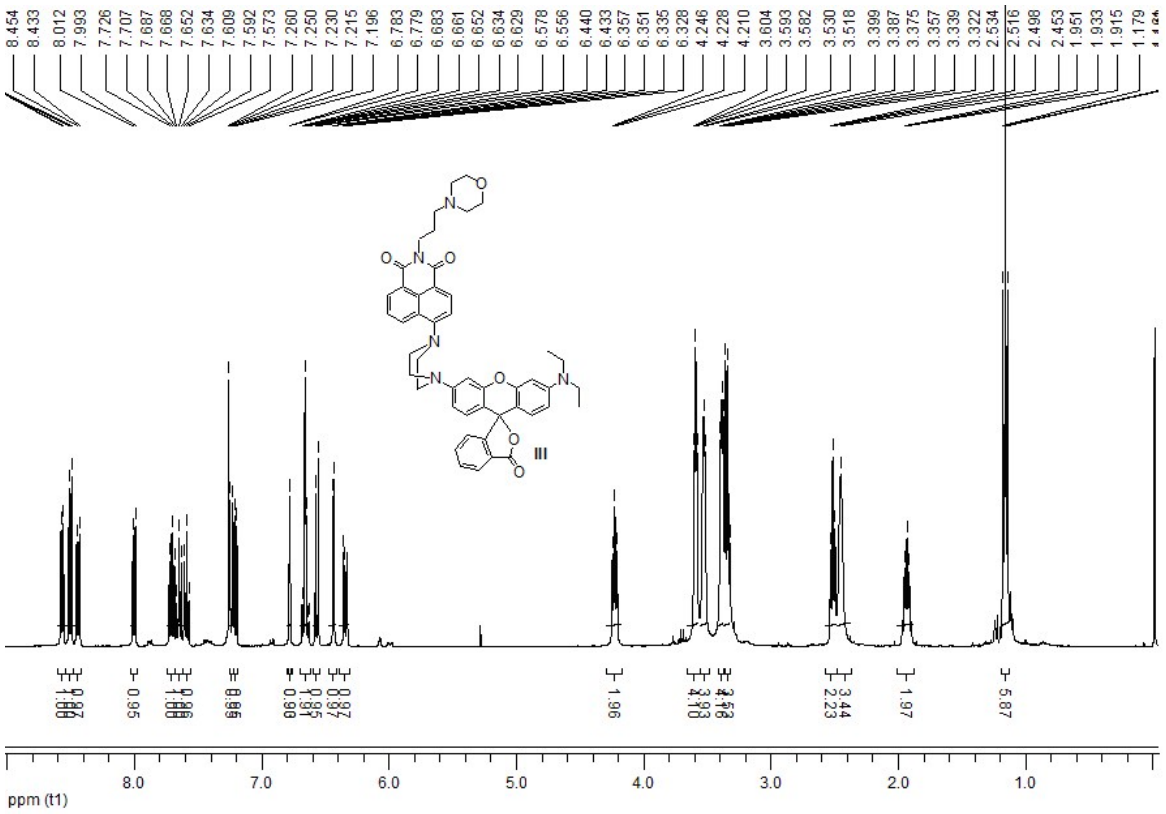

Fig. S18 ^{1}H NMR of **III** (400 MHz, $CDCl_3$).

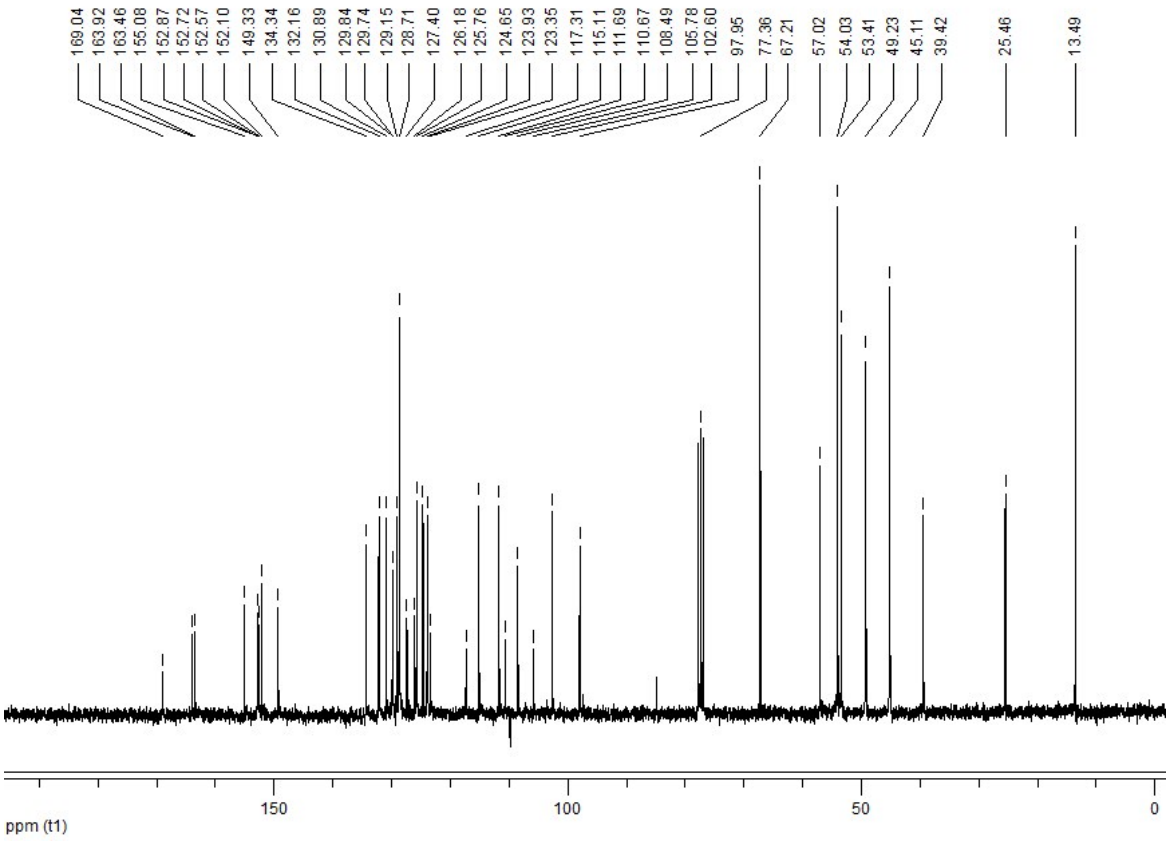

Fig. S19 ^{13}C NMR of **III** (75 MHz, $CDCl_3$).

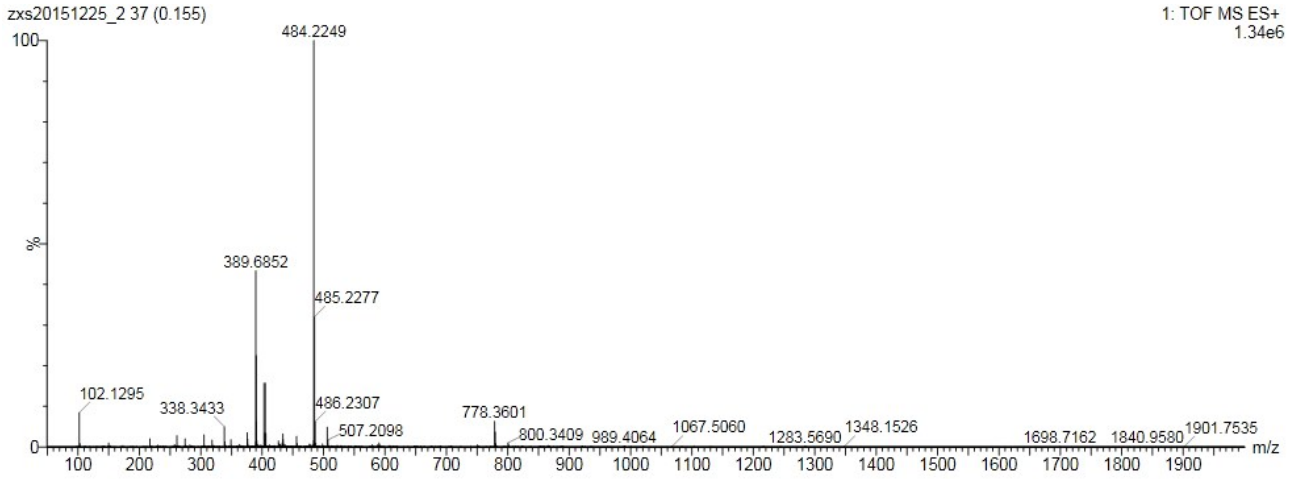

Fig. S20 HRMS (LC/MS) spectra of **III**. The peak at m/z = 778.3601 was assigned to the mass of [**III** + H^+]. The peak at m/z = 389.6852 was assigned to the mass of [**III** + $2H^+$]/2.

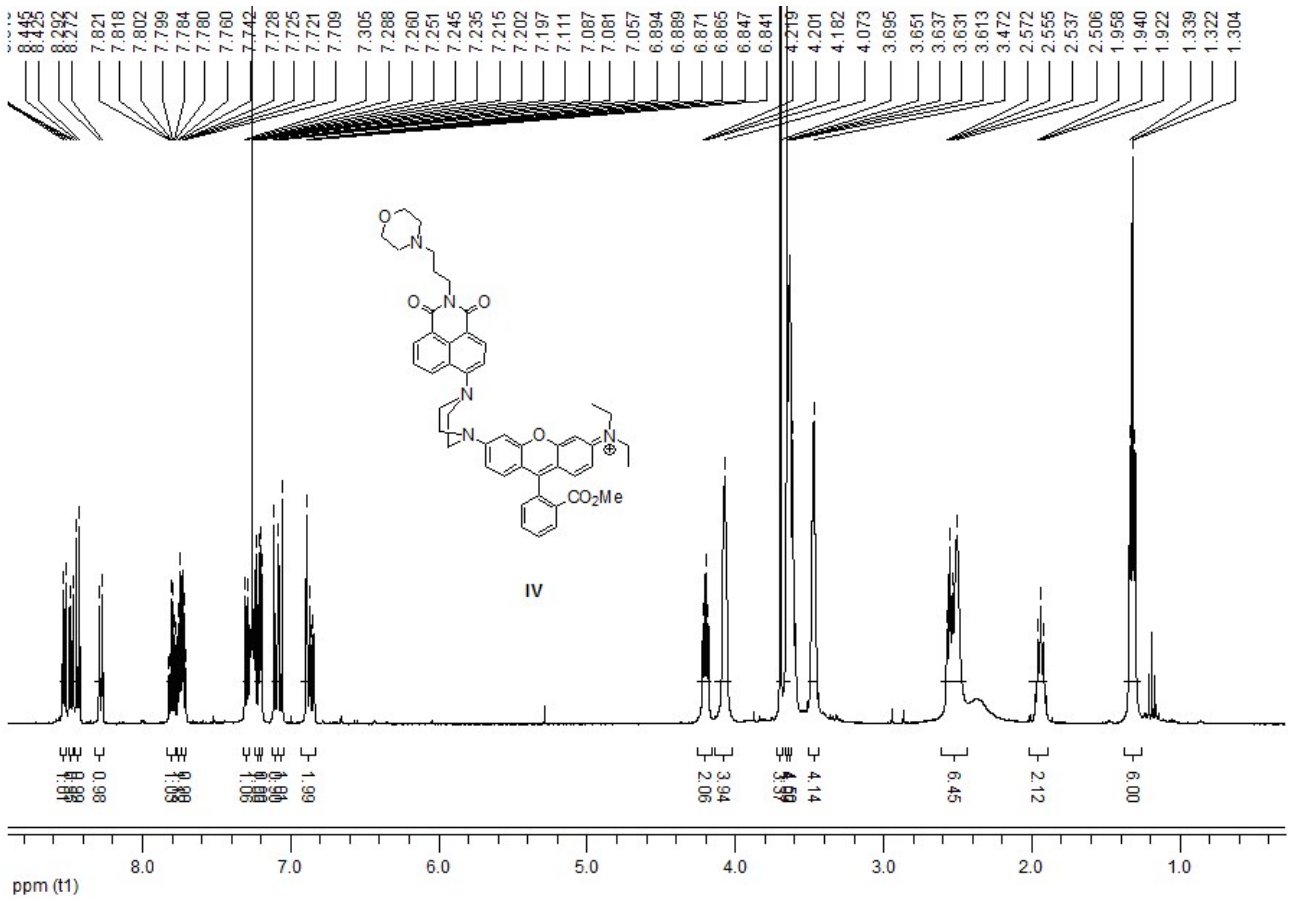

Fig. S21 ^{1}H NMR of **IV** (400 MHz, $CDCl_3$).

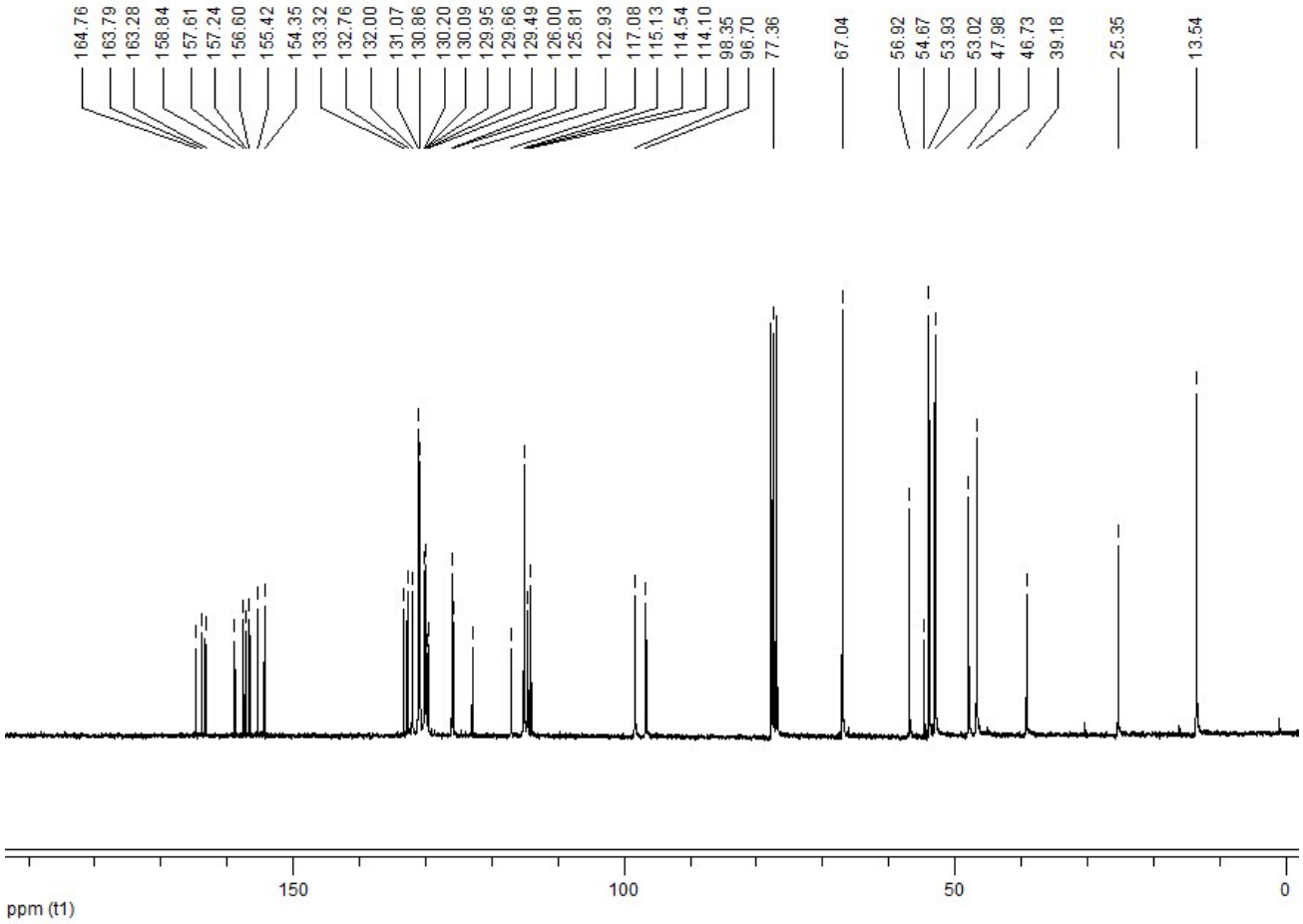

Fig. S22 ^{13}C NMR of **IV** (75 MHz, $CDCl_3$).

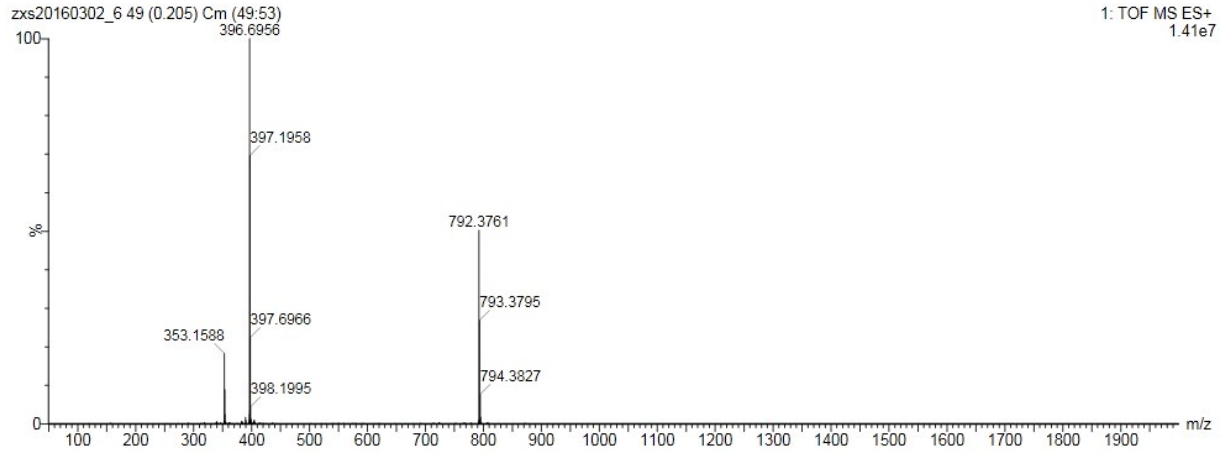

Fig. S23 HRMS (LC/MS) spectra of **IV**. The peak at m/z = 792.3761 was assigned to the mass of [**IV** + H^+], the peak at m/z = 396.6956 was assigned to the mass of [**IV** + H^+]/2.

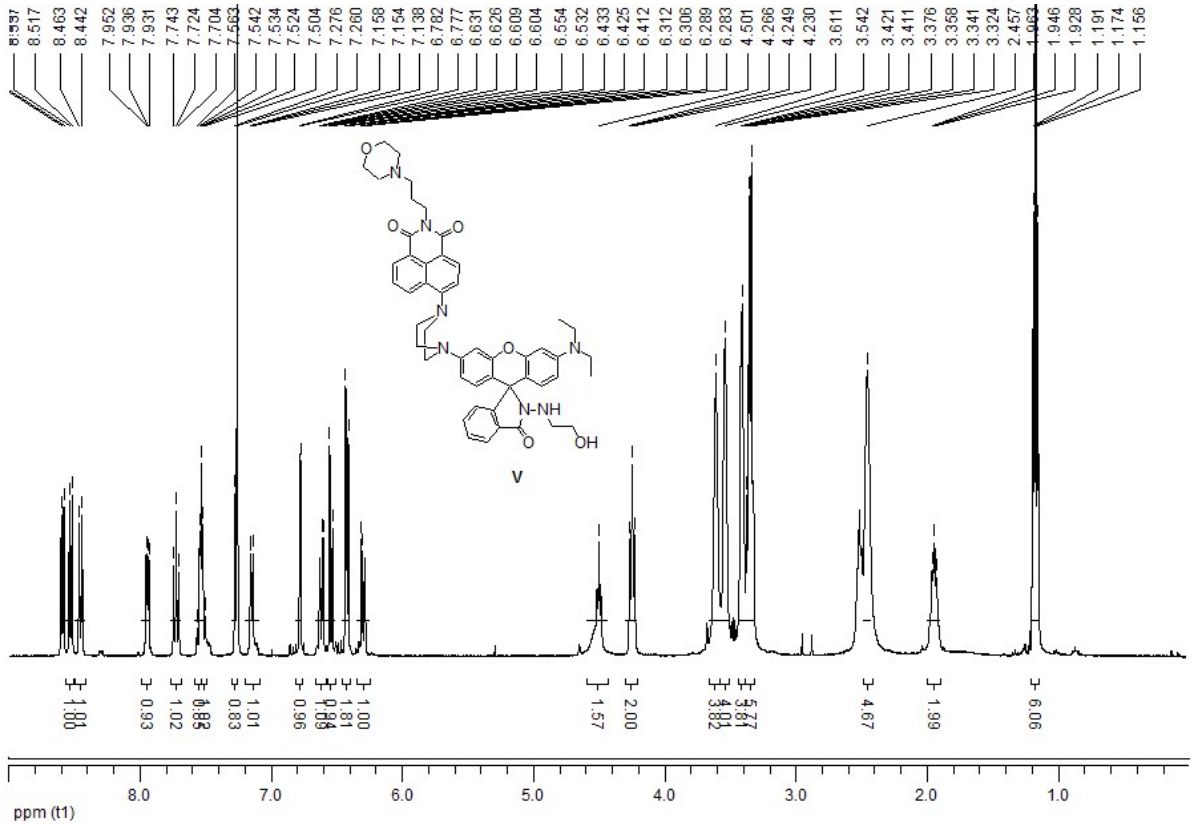

Fig. S24 ^{1}H NMR of **V** (400 MHz, $CDCl_3$).

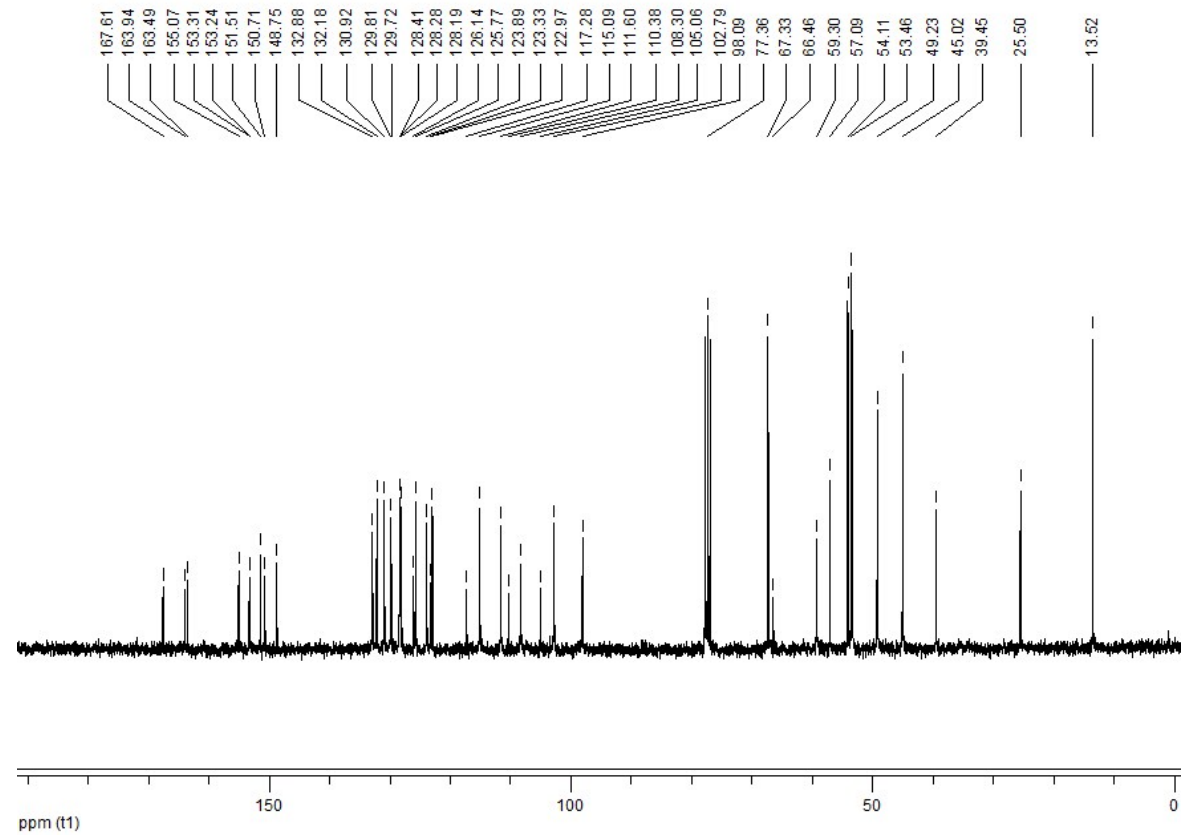

Fig. S25 ^{13}C NMR of **V** (75 MHz, $CDCl_3$).

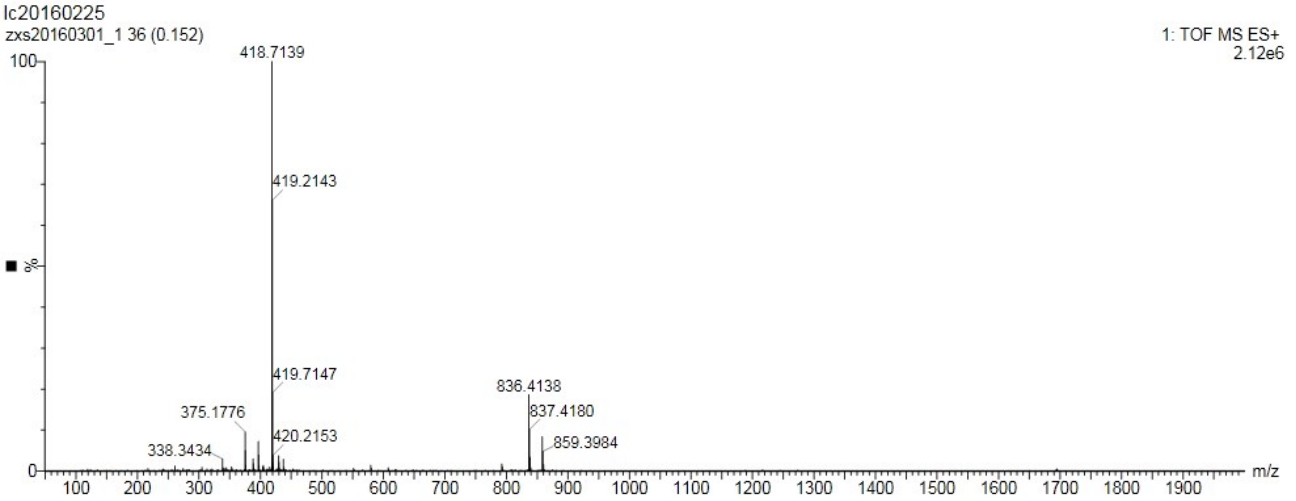

Fig. S26 HRMS (LC/MS) spectra of **V**. The peak at m/z = 836.4138 was assigned to the mass of [**V** + H^+], the peak at m/z = 859.3984 was assigned to the mass of [**V** + Na^+], and the peak at m/z = 418.7139 was assigned to the mass of [**V** + $2H^+$]/2.

References:

[S1] P. Du, S. J. Lippard, *Inorg. Chem*., 2010, **49**, 10753.

[S2] *a*) G. Long and J. Winefordner, *Anal. Chem.,* 1983, **55**, 712A; *b*) S. Pandey, A. Azam, S. Pandey and H. Chawla, *Org. Biomol. Chem.,* 2009, **7**, 269.